International Journal of Legal Medicine (2023) 137:1815–1837
https://doi.org/10.1007/s00414-023-03040-y

ORIGINAL ARTICLE

Sensitivity of temperature-based time since death estimation on measurement location

J. Shanmugam Subramaniam[1] · M. Hubig[1] · H. Muggenthaler[1] · S. Schenkl[1] · J. Ullrich[2] · G. Pourtier[2] · M. Weiser[2] · G. Mall[1]

Received: 24 January 2023 / Accepted: 6 June 2023 / Published online: 19 June 2023

Abstract

Rectal temperature measurement (RTM) from crime scenes is an important parameter for temperature-based time of death estimation (TDE). Various influential variables exist in TDE methods like the uncertainty in thermal and environmental parameters. Although RTM depends in particular on the location of measurement position, this relationship has never been investigated separately. The presented study fills this gap using Finite Element (FE) simulations of body cooling. A manually meshed coarse human FE model and an FE geometry model developed from the CT scan of a male corpse are used for TDE sensitivity analysis. The coarse model is considered with and without a support structure of moist soil. As there is no clear definition of ideal rectal temperature measurement location for TDE, possible variations in RTM location (RTML) are considered based on anatomy and forensic practice. The maximum variation of TDE caused by RTML changes is investigated via FE simulation. Moreover, the influence of ambient temperature, of FE model change and of the models positioning on a wet soil underground are also discussed. As a general outcome, we notice that maximum TDE deviations of up to ca. 2–3 h due to RTML deviations have to be expected. The direction of maximum influence of RTML change on TDE generally was on the line caudal to cranial.

Keywords Temperature-based death time estimation · Heat equation · Finite Element cooling model · Core temperature measurement uncertainty · Death time estimation uncertainty

Introduction

Temperature based death time estimation (TDE) is crucial in homicide investigations. TDE is estimated from core temperature measurement data using the model curve T(t) comprising a priori knowledge of the postmortem rectal temperature decline. The phenomenological approach and the physics-based approach are two different techniques used to generate the model curve T(t). The method of Marshall and Hoare with the Henßge parameters from the Nomogram method (MHH) is a prominent phenomenological approach using a double exponential model with fitted parameters for modeling rectal cooling [1]. Physics-based approaches use the heat transfer equation considering heat exchange mechanisms, cooling conditions and thermal material properties. Finite element (FE) based TDE method (FEM) is a physics-based approach with reasonable computational effort (see e.g. [2–4]). For an extensive overview over temperature based TDE see e.g. [5].

In any TDE method, error quantification is a desideratum as TDE results can lead to acquittal or conviction of suspects. Three different errors exist in FEM such as errors due to space and time discretization, input data errors, and model errors. They lead to the deviation of the TDE value from the actual value. Though several approaches for error estimation exist for TDE e.g. for MHH [6] and for FEM [7] none of them takes into account the uncertainty introduced in TDE due to input data errors caused by variations in the rectal temperature measurement location. The present article tries to close this gap using an FE approach. This does not, however, limit the results to FE TDE methods.

Rectal temperature measurement (RTM) can be performed using approved devices and without the necessity to injure

✉ M. Hubig
Michael.Hubig@med.uni-jena.de

[1] Jena University Hospital - Friedrich Schiller University Jena, Institute of Forensic Medicine, Am Klinikum 1, 07747 Jena, Germany

[2] Zuse Institute Berlin, Takustraße 7, 14195 Berlin, Germany

the body. However, there is a certain amount of diversity in the characterization of the measurement locus in forensic literature. In early well-known TDE studies [8, 9], it is reported a 3 – 4 inches [7 – 10 cm] insertion depth for RTM. Marshall and Hoare [10] mention the relationship between the liver and rectum temperature. Henßge [11, 12] states that the insertion depth for RTM should be at least 8 cm from the musculus sphincter ani. In [11] Henßge estimates the precision of rectal temperature measurement to be about "+-2 °C". Further, Henßge [13] emphasized the usage of linear, rigid and not very flexible thermometers to achieve an insertion depth without applying force. He also recommends a temperature measurement at the mesenteric root in the lower left abdomen additional to the temperature measurement in the deep abdominal space [14]. Moreover, Henßge advises the thermometer to be inserted in the rectum as deep as possible without applying any force [15]. Indeed, a lot of discrepancy in rectal temperature measurement location exists in literature, so it is necessary to study its effects on TDE. Hence, this motivates a sensitivity analysis of TDE with respect to measurement locus.

The study was executed with participation of the Institute of Legal Medicine (IRM) at the University Hospital Jena of the Friedrich-Schiller-University Jena and of the Zuse Institute Berlin (ZIB), an interdisciplinary research institute for applied mathematics and data-intensive high-performance computing.

Additional computation results are presented in the Supplementary Information (SI) associated with the electronic edition of the article available via the website of the journal.

Method

Finite element model

Background information on numerically solving partial differential equations and on FE simulation can be found e.g. in [16].

For one exemplary case of human corpse with a given CT-scan, two different methods were used to generate FE models. In one of the methods, the FE Model (CTM) was developed from the segmentation of a CT scanned human body and in the other, the human body was manually approximated by hexahedral elements (see e.g. [2, 17]). Two variants of this manually generated model were constructed: One model (CM) is floating freely in air and a copy (CMS) of CM is laying firmly on a wet soil substrate. Detailed simulations of physical heat transfer processes generated the rectal temperature curves T(t). The corpse cooling was computed in all of the FE models based on the well known heat transfer Eq. (1), a partial differential equation where c is the specific heat capacity, ρ the mass density, and κ the heat conductivity of the tissue:

$$c\rho\frac{\partial}{\partial t}T = \nabla\cdot(\kappa\nabla T) \tag{1}$$

Heat transfer from the body to the environment across the skin due to convection and surface-to-ambient radiation was captured by a Robin boundary condition with effective heat transfer coefficient γ as given in Eqs. (2), (3) (see e.g. [7]):

$$\gamma = h + 4\epsilon\sigma {T_A}^3 \tag{2}$$

$$n^T\kappa\nabla T = \gamma(T_A - T) \tag{3}$$

Here, T_A is the ambient temperature, h is the heat transfer coefficient, ε is the emissivity and σ is the Stefan-Boltzmann constant. In the CTM developed from the CT scan of a human body, the initial temperature field T_0 defined at time t = 0 satisfies Pennes' Bio-Heat-Transfer-Equation (BHTE) [18]

$$-div(\kappa\nabla T_0) + \rho_b c_b w(T_0 - T_{core}) = 0, \tag{4}$$

where $\rho_b c_b$ is the heat capacity of blood, w is tissue perfusion, and T_{core} is the body core temperature.

In the manually developed FE model CM, the initial temperature field T_0 is defined with a gradient between core and outside elements as in [2] referring to physiology literature.

For reliable comparison between the different models, the equivalent effective heat transfer coefficient was applied to the CTM corresponding to the convection and radiation terms applied on CMS and CM. The model curves T(t) were sampled at the designated nodes C and $SP_R k$ (k = 1,…6) corresponding to the anatomical RTM locations (RTML). The point C was placed at the intended measurement location in the respective FE model, whereas the six points $SP_R k$ (k = 1,…,6) lay on the vertices of an octahedron with radius R. The $SP_R k$ were defined to represent possible locations of a misplaced temperature sensor. If no confusion can arise about the value of R the $SP_R k$ are abbreviated SPi.

Our results consist of maximum deviations ${D_{MAX}}^M$ comparing two cooling curves computed at two locations of RTM's in a specified FE model M = CTM, CM, CMS. The distance ${D_{MAX}}^M$ is defined between the cooling curves $T_C(t)$ and $T_{SPi}(t)$ at the center point C of a measurement point octahedron (see Fig. 4) of radius R and at its vertices $SP_R k$ (k = 1, …, 6). We also computed differences ${D_{MAX}}^{M1,M2} := {D_{MAX}}^{M1} - {D_{MAX}}^{M2}$ of those maximum deviations for two pairs (CM-CMS and CM-CTM)

of different FE models (M1, M2) for all C – SP_Ri pairs. All computations were performed for different constant ambient temperatures T_A and for different octahedra radii R. We also performed all of the computations for each of four Q-ranges, where the first three are Henßges Q-ranges (see e.g. [15]).

CT meshed FE model CTM

All of the modeling work done on the CT meshed FE model CTM was performed at the Zuse Institute Berlin (ZIB). The CT scan of a male corpse of length L = 1.74 m and weight M = 62 kg was segmented in the software AMIRA and the segmented data was converted into an FE model, comprising of 961,234 tetrahedral elements, via the FE-program Kaskade (see e.g. [19]), an in-house code of ZIB. As depicted in Fig. 1, the feet of the corpse were not included in the model and the weight, size and volume of the whole model were scaled according to the scanned corpse dimensions. The segmentation of different body parts was carried out using differences in density and location of different tissue types like bone, fat, bladder, kidney, abdomen, liver, heart, lungs and muscle as seen in Table 1 in the Appendix.. In CTM, skin tissue was not segmented separately from the subcutaneous fat tissue since skin tissue was assumed to have a negligible effect on the TDE. Hence, the skin material properties were not considered in CTM.

Coarse meshed FE model CM

Our coarse meshed FE model CM was already described in several publications [2, 3, 20, 21]. Its mesh was manually constructed using the FE preprocessor Mentat. It consists of approx. 12,000 nodes in approx. 8300 hexahedral elements with trilinear shape functions. The model contains numerous compartments (see Fig. 2) standing for distinct anatomical structures of the body.

Our standard FE model of length L = 1.64 m and mass M = 64 kg was scaled geometrically to a length of L' = 1.74 m and weight of M' = 62 kg, corresponding to the male reference body of our study. The scaling factors are defined as in the Eqs. (5) and (6) where k_1 is linear 1-dim scaling along the body length axis and k_2 is linear 2-dim dilation in the transverse plane [2].

$$k_1 = L'/L \tag{5}$$

$$k_2 = \sqrt{\frac{M' \cdot L}{M \cdot L'}} \tag{6}$$

Generation and scaling of FE mesh and post-processing were performed in MSC's pre- and post-processing tool Mentat.

Further, to investigate the TDE sensitivity on more complex boundary conditions favoring thermal energy transfer from the body core in dorsal direction, a supporting structure or floor is modeled with an hexagonal FE mesh as shown in Fig. 2a. The FE model lies on its back on the support structure defined, presumably causing large differences between C-temperature and temperature at SP4 or SP3, i.e. along y direction. The support structure is defined with the thermal properties of wet soil such as thermal conductivity c = 2 W/m^2K, specific heat κ = 2200 J/kgK, density ρ = 1900 kg/m^3 [22] and emissivity ε = 0.95. The coarse model laying on its back on the support structure is abbreviated CMS, whereas the coarse model without support structure is named CM

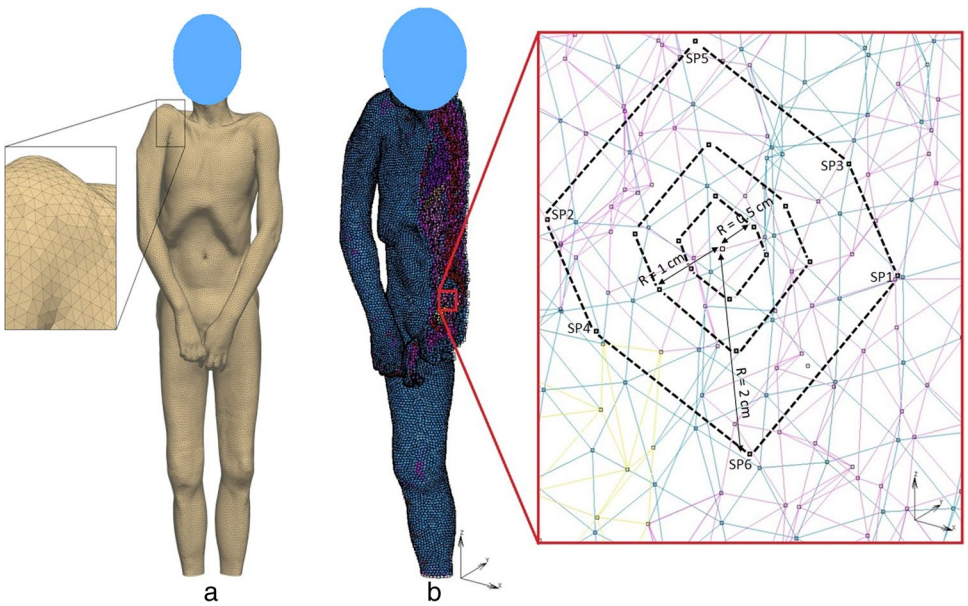

Fig. 1 **a**: CT Meshed male corpse model with magnified mesh detail. **b**: Right half view of CTM model with magnified measurement location showing measurement points C, SPk (k = 1,…,6) in three different octahedra of radii R = 0.5 cm, 1 cm, 2 cm. For the octahedra see Fig. 4. Only the contour lines of the octahedra are shown for clarity

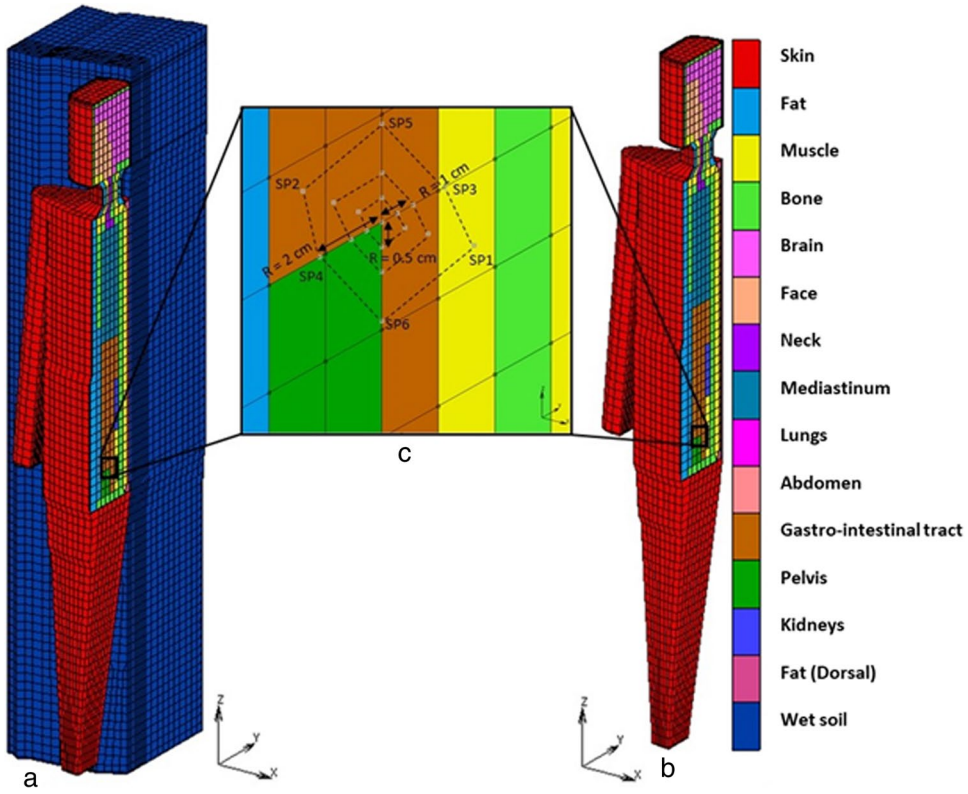

Fig. 2 **a**: Coarse model lying on a support structure (CMS), **b**: Coarse model without support structure (CM), **c**: Detailed view of measurement points C, SP_1,…,SP_6 along different radii R = 0.5 cm, 1 cm, 2 cm. For the octahedra see Fig. 4. Only the contour lines of the octahedra are shown for clarity

(see Fig. 2c). CMS and CM were scaled to the same height and weight as CTM. This will eliminate the influence of weight on the body cooling.

Definition of measurement positions C and SP_Rk

TDE estimations are usually based on a single RTM. Hence, the measurement position is subject to variations due to different anatomies, thermometer angles and insertion depth. An approximate ideal measurement position can be specified from anatomy including forensic knowledge on measurement locations used in practice. The central position C for our measurements was determined in the pars ampullaris of the rectum near the incisura transversalis, which is the passage from pars ampullaris to the pars sacralis of the rectum (Fig. 3).

Additional measurement positions SP_Rk (k = 1, …,6) for our sensitivity studies were chosen in spatial x, y and z direction at distances (octahedral radii) R = 0.5 cm, 1 cm, 2 cm from the central measurement position C. For each fixed distance R six additional measurement locations SP_Rk were established. The six additional measurement positions SP_Rk form an octahedron with the central point C in its middle. The schematic sketch representing the additional positions in the model was illustrated in Fig. 4.

The anatomical position of additional measurement points in CTM are described as follows: SP1 lies in the center of abdomen surrounded by abdomen tissues, SP3 lies nearby bone, SP4 lies in the center of abdomen, SP6 lies very near to abdomen. Figure 1b shows the anatomical positions of measurement points in CTM. Similarly, the anatomical position of additional measurement points in CMS and CM are depicted in Fig. 2c, which helps to identify the position of additional measurement points. SP1 lies lateral from C in positive X direction. Due to CM's left–right symmetry the temperature value at SP2 is equal to the temperature at SP1. The points SP2, SP3, SP5 lie in the gastrointestinal tract. SP6 and SP4 lie on the border between gastrointestinal tract and pelvis.

Simulation

The CT-generated model CTM was imported from the FE research code Kaskade 7 [19] into the commercial MSC-Marc Mentat FE system and the material parameters are defined as given in Table 1 of [2] (see Table 1 in the Appendix). The same material properties were used also for CMS and CM models. The initial temperature field $T_0(r)$ at the time of death on the body was calculated via the Pennes' Bio-Heat-Transfer-Equation BHTE on the original CTM model [18]. The field $T_0(r)$ was approximated by 10 discrete node sets corresponding to 10 discrete temperatures in the converted version of CTM. In the CMS and CM models, the initial temperature was defined

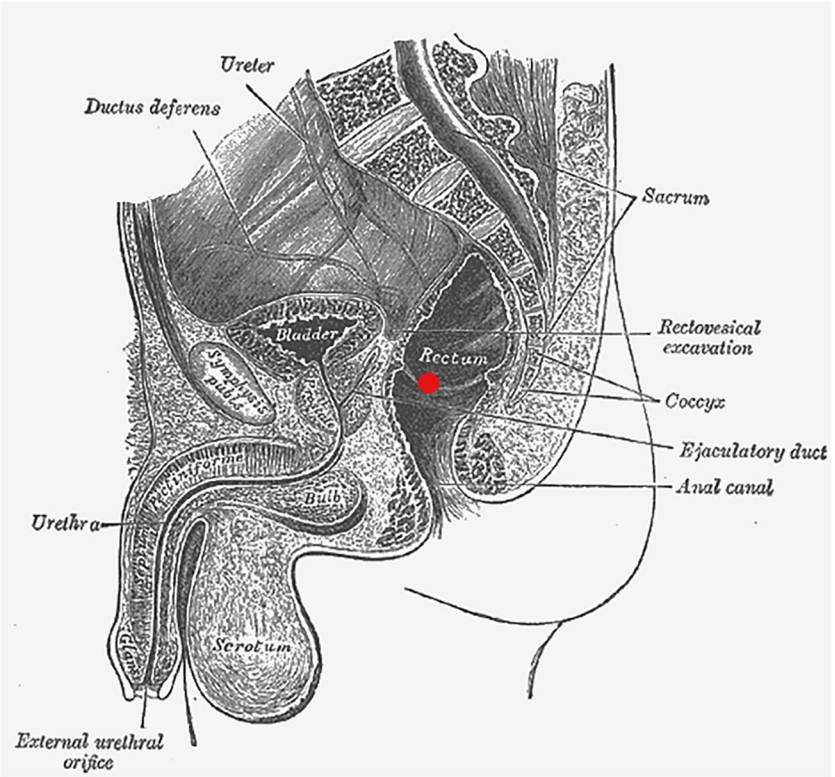

Fig. 3 Anatomical sketch depicting ideal measurement location [23]

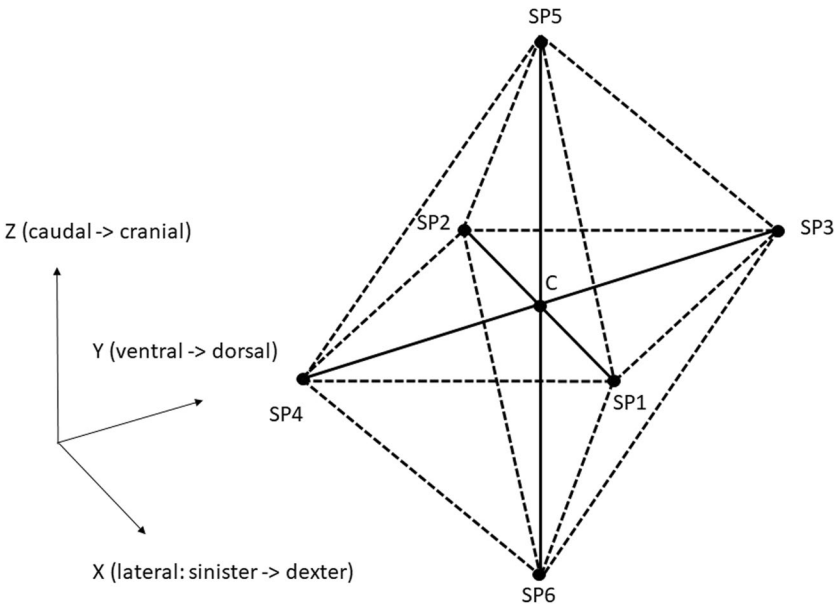

Fig. 4 Central position C and six additional measurement positions ($SP_R k =$) SPk (k = 1,…,6) in X, Y and Z direction in CTM, CMS, CM model at different radii R = 0.5 cm, 1 cm, 2 cm from center position C

according to [2] where it was taken from physiological textbooks. The simulation is carried out for three different constant ambient temperatures $T_A = 5°$ C, 15° C, 25° C. The convection and radiation parameters in CTM were defined by the effective heat transfer coefficient $\gamma = 4 \bullet \varepsilon \bullet \sigma T_A^3$ [7] and the calculated values in increasing order of $T_A = 5°$ C, 15° C, 25° C are $\gamma = 7.93$ W/m^{2}K, 8.45 W/m^{2}K, 9 W/m^{2}K. In CMS and CM, a convection coefficient of $h = 3.3$ W/m^2 K is applied [2]. Radiation view factors in the CMS and CM models were computed by Monte-Carlo-simulation [2]. Although the method of defining boundary conditions differs between CTM and CM models, it was found that the linearization of the radiation term applied in CTM has negligible effect on the cooling curve [7]. A

sparse direct algorithm in MSC-Marc 2020 and adaptive time stepping with maximum allowed temperature change of 1°K and 0.1 s initial time step were used.

Quantification of TDE deviations

TDE deviation from the central position C to any position $SP_R k$ is quantified by the maximum distance D_{MAX} between the respective cooling curves, which is defined in this section. Let the time interval [a, b] be given during body cooling which starts at 0 h and let a = 1 h be the left point and b = 45 h be the right point of our interval. Let further $T_1(t)$ and $T_2(t)$ be two cooling curves defined on the interval [0, b]. Evaluation of the cooling curve distances started at a > 0 h for reasons of numerical stability. The ambient temperature T_A is assumed constant in space and time outside the body. The *reference curve* $T_R(t)$ for two cooling curves $T_1(t)$ and $T_2(t)$ is constructed as the pointwise mean of $T_1(t)$ and $T_2(t)$:

$$\forall t \in [a,b] : T_R(t) := (T_1(t) + T_2(t))/2 \tag{7}$$

Let $T_0 := T_R(0)$ be the initial temperature at the center point C. Now the reference curve $T_R(t)$ can be normalized to the function Q(t) taking values in the real number's interval [0, 1]:

$$\forall t \in [a,b] : Q(t) := (T_R(t) - T_A)/(T_0 - T_A) \tag{8}$$

This makes it possible to define the Q-intervals Q_1 to Q_4 (where Q_1, Q_2, Q_3 correspond to Henßge's [15] normed temperature ranges for tolerance radii) and their left and right boundaries q_0, …, q_4 by:

$$q_0 := 1, q_1 := 0.5, q_2 := 0.3, q_3 := 0.2, q_4 := 0.1 \tag{9}$$

$$\forall 1 \le n \le 4 : Q_n :=]q_{n-1}, q_n] \tag{10}$$

Assuming $T_R(t)$ to be strictly monotonically decreasing, we can uniquely map the Q-interval boundaries q_n to the respective temperature values $T_{R(4-n)}$.

$$\forall 0 \le n \le 4 : T_{R(4-n)} := q_n \cdot (T_0 - T_A) + T_A \tag{11}$$

Since the two cooling curves T_1 and T_2 are monotonically decreasing it is possible to define their inverse curves t_1, t_2, called the **(absolute) time since death (TSD) estimation result curves** w.r.t. the cooling curves T_1, T_2 on the domain $[T_{MIN}, T_{MAX}]$ which is the range of the reference curve T_R on the temperature axis by:

$$t_1 : [T_{MIN}, T_{MAX}] \to IR : (T \to t_1(T) := T_1^{-1}(T)) \tag{12}$$

$$t_2 : [T_{MIN}, T_{MAX}] \to IR : (T \to t_2(T) := T_2^{-1}(T)) \tag{13}$$

The time functions t_1, t_2 are frequently concatenated with the reference curve T_R, thus giving $t_1(T_R(t))$, $t_2(T_R(t))$ in the following definitions. For short those concatenations will be abbreviated $t_1(t)$, $t_2(t)$. If the point t in time is clear, we will even write t_1, t_2. We will now quantify the distance between the cooling curves T_1 and T_2, which are actually constructed as distances between the inverse curves t_1 and t_2. The reason for this construction lies in our primal interest in time differences because our research's number one target is *time since death*. All of the temperature curve distance measures are constructed using the (time oriented!) maximum distance $D_{MAX}(T_1,T_2)$ between two cooling curves T_1 and T_2, which is shown here for continuous functions first. The maximum domain of the reference curve T_R on the time axis is the interval $[t_{MIN}, t_{MAX}]$ which is taken therefore as the domain for maximum-finding in our definition:

$$D_{MAX}(T_1, T_2) := max_{t \in [t_{MIN}, t_{MAX}]} \left| t_1(T_R(t)) - t_2(T_R(t)) \right| \tag{14}$$

We will now consider the equivalent of the definition (14) in terms of real measured temperature curves $T_i(t)$. Each curve $T_i(t)$ is represented as a finite series of real measurement values $(T_i^1, \ldots, T_i^N)$ on a finite (regular) grid of time values $(t^1, \ldots, t^N)$ which is the same for both of the curves. The first point t^1 of the time grid is identical to the starting time of cooling computation, while the last point t^N marks the end of the cooling computation interval. To provide a joint domain of definition for both our inverted temperature curves T_R^{-1} we define:

$$T_{MAX} := min\{T_1^1, T_2^1\} \tag{15}$$

$$T_{MIN} := max\{T_1^N, T_2^N\} \tag{16}$$

Now we have constructed the range of our reference curve $T_R(t)$. The limits of its domain of definition $[t_{MIN}, t_{MAX}]$ were computed:

$$t_{MIN} := T_R^{-1}(T_{MAX}) \tag{17}$$

$$t_{MAX} := T_R^{-1}(T_{MIN}) \tag{18}$$

Let K be a natural number and let $(t^1, \ldots, t^K)$ be a regular time grid on the interval $[t_{MIN}, t_{MAX}]$ with $t^1 := t_{MIN}$ and $t^K := t_{MAX}$. This provides the equidistant sampling points for the final definition of the functions $t_i(T_R(t))$. Let further be $(T^1, \ldots, T^K)$ the corresponding temperature grid with $T^1 \le \ldots \le T^K$ and $T^k := T_R(t^k)$ for all k = 1, …, K and $T^K := T_{MAX}$. The time grid's width Δt is:

$$\Delta t := \frac{t_{MAX} - t_{MIN}}{K - 1} \tag{19}$$

Let further be t_{qn} the inverse image of T_{Rn} under the reference function T_R for all n = 0, …, 4:

$$\forall 0 \le n \le 4 : t_{qn} := T_R^{-1}\left(T_{R(4-n)}\right) \quad (20)$$

The five points t_{qn} on the time scale constitute the endpoints of four time intervals t_{Q1}, …, t_{Q4}:

$$\forall 1 \le n \le 4 : t_{Qn} :=]t_{qn-1}, t_{qn}] \quad (21)$$

We will redefine our measure (14) quantifying the distance between the cooling curves T_1 and T_2 in terms of the real samples $(t^1, \ldots, t^K)$ and $(T_i^1, \ldots, T_i^K)$. The distance measure is the distance $D_{MAX}(T_1, T_2)$. It is defined in a global version on the whole time interval $[t_{MIN}, t_{MAX}]$ and in four local ones residing on one of the intersections $t_{Qj} \cap [t_{MIN}, t_{MAX}]$ on the time axis each. For all $1 \le i \le 4$ the number of t^k lying in $t_{Qj} \cap [t_{MIN}, t_{MAX}]$ is denoted by K_i.

The *(absolute global) maximum distance* $D_{MAX}(T_1, T_2)$ is defined as:

$$D_{MAX}(T_1, T_2) := max_{1 \le k \le K} |t_1(T_R(t^k)) - t_2(T_R(t^k))| \quad (22)$$

while the *(absolute) Q_i-local maximum distance* $D_{MAX,Qi}(T_1, T_2)$ is defined for i = 1, …, 4:

$$D_{MAX,Q_i}(T_1, T_2) := max_{1 \le k \le K_i, t^k \in t_{Qi} \cap [t_{MIN}, t_{MAX}]} |t_1(T_R(t^k)) - t_2(T_R(t^k))| \quad (23)$$

Results

In a first step we evaluated the results for the direction in space (X,Y,Z as in Fig. 4), where the largest TDE-deviation value D_{MAX} caused by RTML -variation was seen. Interestingly, this *maximum direction depended neither on the ambient temperature T_A = 5 °C, 15 °C, 25 °C nor on the octahedron radius R = 0.5 cm, 1 cm, 2 cm*. The FE-model chosen makes the only difference. Therefore we get the following list of directions for maximum D_{MAX} caused by RTML-variation:

- CM: Z caudal—cranial
- CTM: Y ventral—dorsal
- CMS: Y ventral—dorsal

TDE deviations measured by D_{MAX}^{M} on the FE model M = CTM, CMS, CM respectively depending on ambient temperature T_A and measurement radius R are represented in Figs. 5, 6 and 7. The differences of TDE deviations $D_{MAX}^{M1,M2}$ on the model pairs (M1, M2) = (CM, CTM), (CM, CMS) as depicted in Figs. 8 and 9 were calculated as follows: $D_{MAX}^{CM,CTM} = D_{MAX}^{CM} - D_{MAX}^{CTM}$ and $D_{MAX}^{CM,CMS} = D_{MAX}^{CM} - D_{MAX}^{CMS}$.

TDE deviations $D_{MAX,Qi}^{M}$ at various measurement points $SP_R k$ (k = 1, …,6) evaluated against C in M = CTM, CMS,

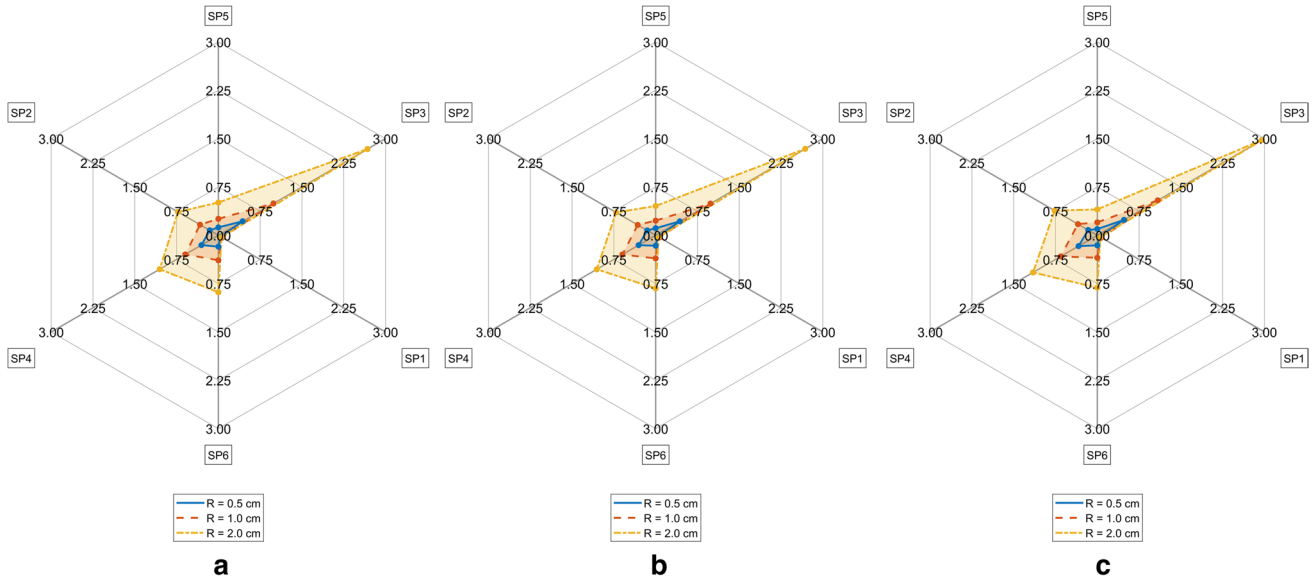

Fig. 5 TDE deviation in D_{MAX} for CTM for R = 0.5 cm (Solid line), R = 1.0 cm (Dashed line), R = 2 cm (Dash-dotted line) **a**. T_A = 5° C, **b**. T_A = 15° C, **c**. T_A = 25° C

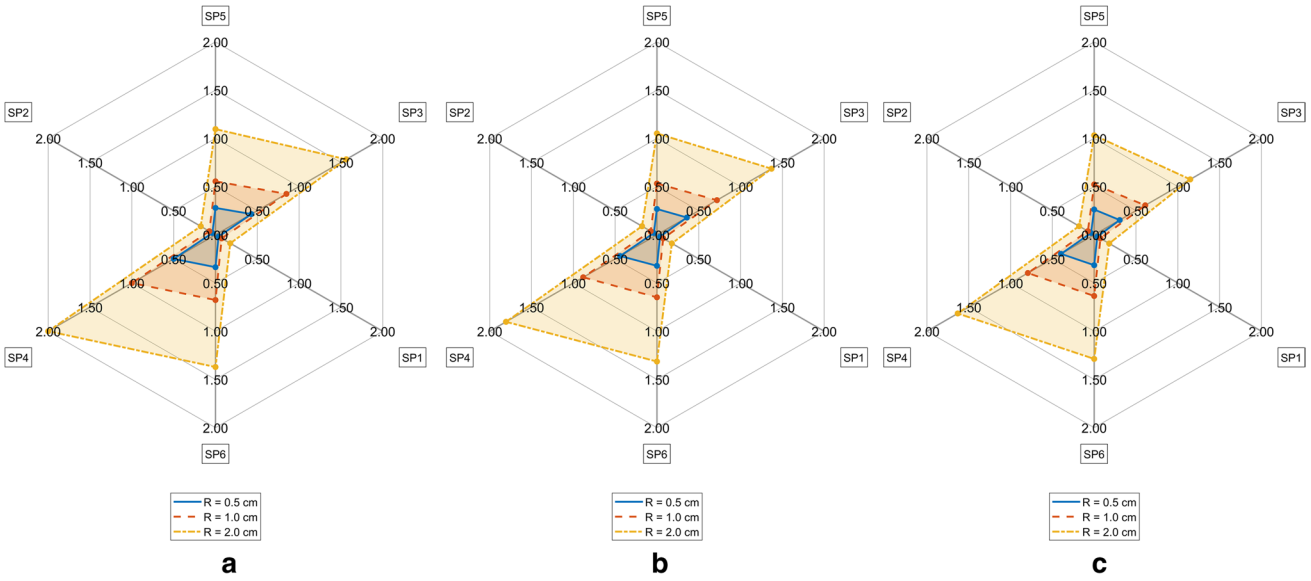

Fig. 6 TDE deviation in D_{MAX} for CMS for R = 0.5 cm (Solid line), R = 1.0 cm (Dashed line), R = 2 cm (Dash-dotted line) **a**. $T_A = 5°$ C, **b**. $T_A = 15°$ C, **c**. $T_A = 25°$ C

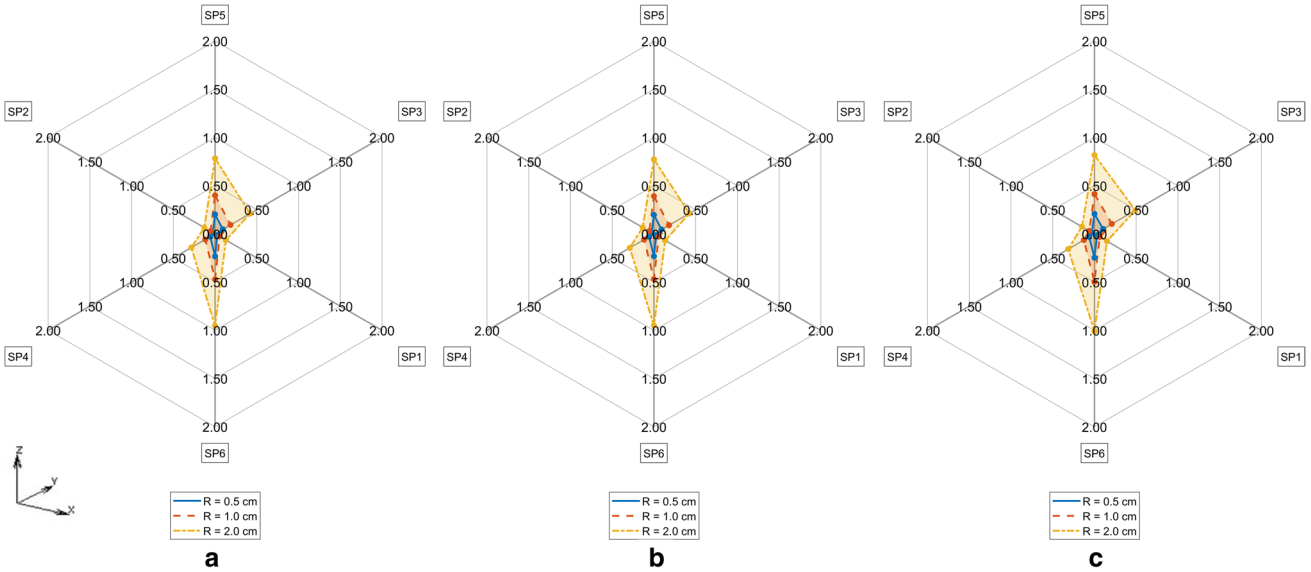

Fig. 7 TDE deviation in D_{MAX} for CM for R = 0.5 cm (Solid line), R = 1.0 cm (Dashed line), R = 2 cm (Dash-dotted line) **a**. $T_A = 5°$ C, **b**. $T_A = 15°$ C, **c**. $T_A = 25°$ C

CM at various ambient temperatures T_A and Q regions are shown in Tables 2, 3, 4, 5, 6, 7, 8, 9 and 10 in the Appendix. The RTML $SP_R k$ (k = 1, …,6) in Tables 2, 3, 4, 5, 6, 7, 8, 9 and 10 are arranged corresponding to clockwise order in Figs. 5, 6, 7, 8 and 9. Browsing the tables the following regularities can be noticed:

(R1) For all of the models M = CTM, CMS, CM, and for each fixed combination of T_A and R the maximum value of $D_{MAX,Qi}$ over all Qi and over all $SP_R k$ is taken at $SP_R 4$ in Q1 (dark grey, fat print in Tables 2, 3, 4, 5, 6, 7, 8, 9 and 10).

(R2) For M = CM, CMS, and for each fixed combination of T_A, R, $SP_R k$ the maximum value of $D_{MAX,Qi}$ over all Qi is taken in Q1 (light grey in Tables 5, 6, 7, 8, 9 and 10).

(R3) For M = CTM, and for each fixed combination of T_A, R, the maxima of $D_{MAX,Qi}$ for fixed $SP_R k$ are as follows:

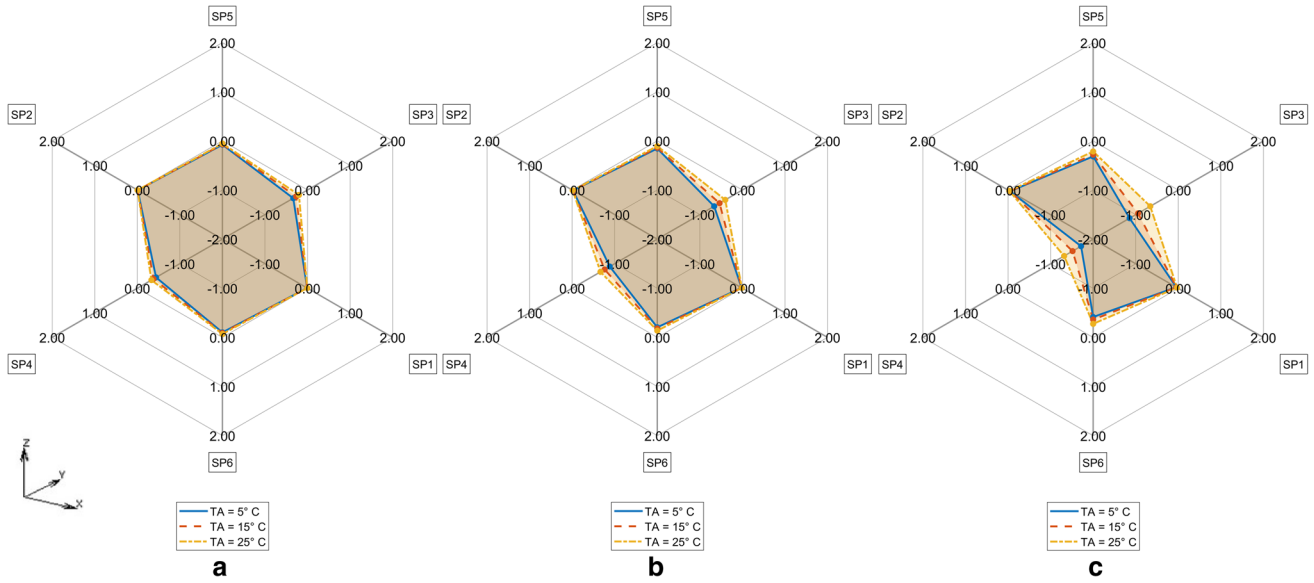

Fig. 8 Difference in TDE deviation in D_{MAX} between CM vs CMS model for $T_A = 5°$ C (Solid line), $T_A = 15°$ C (Dashed line), $T_A = 25°$ C (Dash-dotted line) for **a**. R = 0.5 cm, **b**. R = 1 cm, **c**. R = 2 cm

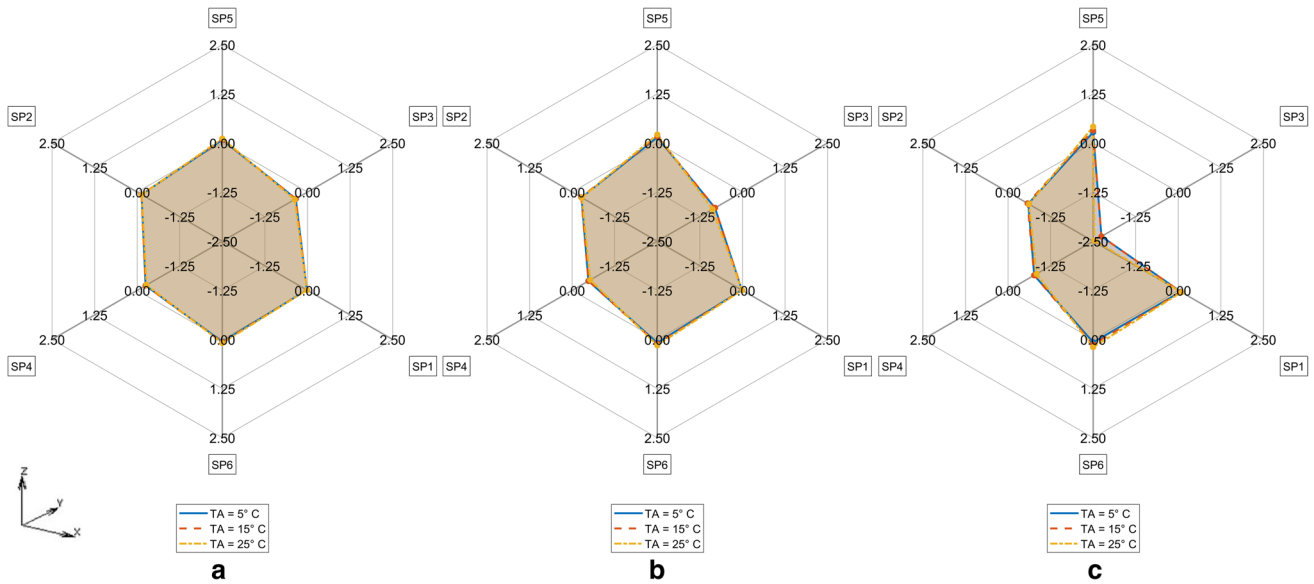

Fig. 9 Difference in TDE deviation in D_{MAX} between CM vs CTM for $T_A = 5°$ C (Solid line), $T_A = 15°$ C (Dashed line), $T_A = 25°$ C (Dash-dotted line) **a**. R = 0.5 cm, **b**. R = 1 cm, **c**. R = 2 cm

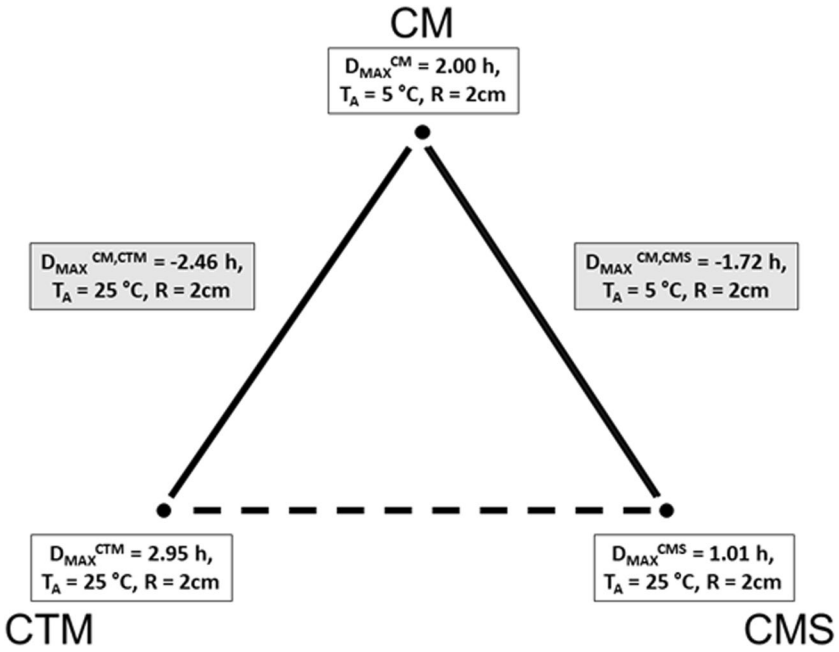

Fig. 10 Maximum TDE deviation in D_{MAX} in CTM, CMS and CM model

a In the SP_R5- and in the SP_R3-column at Q2
b In the SP_R1- and in the SP_R6-column at Q4
c In the SP_R2-column at Q1

(R4) For M = CM, CMS, and for each fixed combination of T_A, R, SP_Rk the $D_{MAX,Qi}$ values are declining with rising index i of Q_i. The only exception occurs for M = CMS in Table 7 and $T_A = 25$ °C at R = 1 cm and R = 2 cm at SP_R3: where we see $D_{MAX,Qi}$ rise from Q3 to Q4

Results concerning relative TDE difference distances and distances based on the L_2-norm instead of the MAX norm are presented in the electronic SI.

Discussion

Multiple analysis was carried out to determine the TDE error caused by measurement locus variations for the different FE-model types such as CTM, CM, CMS using maximum distance D_{MAX}.

Our simulation results show maximum TDE deviations D_{MAX} with respect to variations in RTML up to 2 cm in the order of magnitude of 2 to 3 h. Comparing to other influences like variations in ambient temperature T_A (see [6, 7]), initial body core temperature T_0 (see [20]), etc. the TDE deviations of 2 to 3 h are not negligible and can cause considerable errors in TDE. Our RTML-caused TDE deviation results D_{MAX} lie within the 95% confidence interval of Henßge [15]. For the first Q interval, Henßge gives a value of 2.8 h for standard as well as for non-standard conditions, which is in the same order of our TDE deviations caused by variations of the RTML.

The maximum TDE deviation D_{MAX} in CTM and in CMS is observed in the dorsal–ventral axis Y (Fig. 5: SP3, Fig. 6: SP4).

This may be due to the close vicinity of RTML to backbone tissue. A higher value of thermal conductivity of bone tissue of k = 0.75 W/m^{2}K compared to the conductivity of other soft tissue types, will result in higher temperature gradient in the line C – nearest backbone parts. Similarly, a higher temperature gradient occurs along the Y: dorsal–ventral SP3—C—SP4 axis in case of CMS due to high conductivity of substrate. Only in CM the axis SP6 – C – SP5 (Z: caudal—cranial) shows the highest D_{MAX} values (see Fig. 7). This may be the case because the CM model lacks the high conductivity substrate the CMS model contains. Other differences between CM and the other models might as well be part of the explanation: The CM shows symmetric anatomical structures with respect to the mid sagittal plane while the CTM does not. Furthermore, the CTM has a much finer discretization than the CM and a varying spatial tissue distribution due to the manual versus the CT-based mesh generation in CM and CTM respectively. Concerning the FE-meshwidth, we found only a minor effect on the TDE difference results as well as [7]. Hence, the TDE differences between the CM and the CTM can hardly be explained from differences in the discretization order.

The only difference between CMS and CM is that in CMS, the coarse-meshed human model lies on a discretized structure with wet soil's thermal properties whereas CM consists of a coarse-meshed human model floating

freely (like CTM model) in air without contact to other solid structures. The difference $D_{MAX}^{CM,CMS}$ compares CM vs. CMS model thus considering the influence of the support structure on the sensitivity of TDE against RTML variation. Like in forensic scenarios heat transfer from the corpse to support with high conductivity and / or heat capacity will increase heat flux through the models support-contact faces. Assuming a support with comparably low thermal conductivity, like a highly insulated mattress, a decrease in heat flux will be the consequence. The influence of different support materials on TDE was investigated in [21, 24]. Thermal properties of the support were also considered in the Henßge model, where supports with high thermal conductivities are taken into account by increasing the correction factor and vice versa (see e.g. [15]). Our results show that the influence of different supports on TDE sensitivity with respect to RTML variations need to be considered because they may lead to differences in temperature gradients which transform to differences in TDE.

The ambient temperature T_A influences the TDE sensitivity against RTML variations in the CMS model in such a way that the TDE deviation increases with decrease in T_A. Possibly, this effect is due to the presence of the support structure along the dorsal–ventral axis (Y axis (SP4 – C – SP3)), which increases the rate of heat transfer. The initial temperature of the support structure was always set to the ambient temperature T_A. In contrast, looking at the TDE difference $D_{MAX}^{CM,C_{TM}}$ between D_{MAX} in CM and in CTM, there is nearly no influence of ambient temperature T_A. Apparently, the influence of T_A on TDE difference is more profound when the support structure is present.

Concerning the influence of RTML variation radius R, the maximum TDE deviation D_{MAX} increases with increase in R in CTM, CMS and CM. This is due to greater Euclidean distance of measurement points from the actual measurement point, which is translated via temperature gradient to greater D_{MAX}.

Figure 10 gives the overview of the maximum TDE deviation by RTML variation evaluated by D_{MAX} for CTM, CMS and CM with respect to ambient temperature T_A and measurement variation radius R.

The evaluation of the Qi-located TDE distances $D_{MAX,Qi}^{M}$ between SP_Rk and C yields the following results: Firstly measurement location errors in the ventral –dorsal axis Y seem to cause the most severe deviations of TDE (see (R1)). For the coarse model regardless of whether there is a wet soil substrate (M = CMS) or not (M = CM) the $D_{MAX,Qi}$ values essentially decline with rising Q-index I that is for rising cooling times (see (R4)). Since the latter regularity is not repeated by the CT-generated model CTM, we infer this to be an artificial effect caused by the unrealistic high symmetry and regularity of the 'hand-crafted' FE models CMS and CM. Generally the effect of RTML errors on TDE seems to be highest at short times after death (see (R1)). Time evolution of TDE errors due to RTML variations thus correspond to the well known effect, that initial temperature deviations lead to high TDE errors during short times p.m. but are later damped to a low constant basic amount. This is shown in [6] for MHH – TDE but may be generalized. Moreover it is consistent with [7].

There are limitations of the current study. Firstly, we used a simulation-based approach for TDE estimation and RTML variation. A validation of our results on experimental measurements with real corpses was not realized. Measurements using corpses of recently deceased – aside from rare availability of such corpses—are difficult to carry out and especially a reproducible RTML variation is nearly impossible. However, in former studies the CM was calibrated and validated based on some experimental measurements published in [21]. Due to the physics-based approach, both the CM and the CTM should be suitable to carry out parameter variations in terms of RTML variation. Secondly, we only use three different models with normal body mass index. Cooling scenarios with more complex boundary conditions, like adipose corpses, clothing and coverings, etc. were not considered although these factors can influence TDE deviation as CMS depicts. Since varying all those boundary conditions would exceed the scope of one research article, those sensitivity studies are left for future research.

Conclusions

TDE variations caused by RTML deviations may be a source of error in legal medicine TDE since they may reach a magnitude of 2–3 h. A possible consequence for legal medicine applied research could be to investigate methods and devices for reproducible RTML determination.

Appendix

Table 1 Material properties used in CTM, CM and CMS model [Mall 2005A]

	CTM, CM and CMS model		
Property	Conductivity	Capacity	Density
Unit	W/mK	J/kgK	Kg/m^3
Skin	0.47	3680	1085
Fat	0.21	2300	920
Muscle	0.51	3800	1085
Bone	0.75	1700	1357
Brain	0.49	3850	1080
Face	0.51	3245	1056
Neck	0.48	3363	1006
Median intestinal Organs	0.47	3375	1033
Lungs	0.28	3520	560
Stomach	0.48	3730	1080
Abdomen	0.46	3346	933
Bladder	0.49	3350	1008
Kidney	0.39	3158	1026
Fat back	0.21	2300	920
Wet soil	2	2200	1900

Table 2 TDE deviation $D_{MAX}{}^{M}$ in M = CTM at $T_A = 5°$ C. Maximum value for fixed R and fixed SP_Rk: light grey, maximum value for fixed R over all SP_Rk: fat print, dark grey

TDE deviation – CTM model - D_{MAX}						
TA = 5° C, R = 0.5 cm						
	SP5	SP3	SP1	SP6	SP4	SP2
Q1	0.122852	0.093391	0.072357	0.055339	**0.435910**	0.386072
Q2	0.373923	0.369764	0.044560	0.038094	0.034864	0.032667
Q3	0.176460	0.141712	0.120125	0.103497	0.303744	0.270017
Q4	0.262275	0.260607	0.155169	0.134974	0.127751	0.123630
TA = 5° C, R = 1 cm						
Q1	0.255475	0.191303	0.145863	0.109616	**0.989255**	0.875922
Q2	0.843773	0.833404	0.070145	0.059609	0.054310	0.050870
Q3	0.387430	0.311325	0.265372	0.231326	0.593254	0.527706
Q4	0.511466	0.507438	0.329621	0.286434	0.270129	0.261497
TA = 5° C, R = 2 cm						
Q1	0.508475	0.368379	0.273719	0.200823	**2.676332**	2.381748
Q2	2.272005	2.236726	0.055936	0.045853	0.040050	0.036235
Q3	0.884038	0.707707	0.604823	0.533477	1.038491	0.925452
Q4	0.898327	0.891724	0.724933	0.628021	0.586598	0.566291

Table 3 TDE deviation $D_{MAX}{}^{M}$ in M = CTM at $T_A = 15°$ C. Maximum value for fixed R and fixed SP_Rk: light grey, maximum value for fixed R over all SP_Rk: fat print, dark grey

TDE deviation – CTM model - D_{MAX}						
TA = 15° C, R = 0.5 cm						
	SP5	SP3	SP1	SP6	SP4	SP2
Q1	0.109587	0.092683	0.070249	0.055203	**0.433453**	0.421614
Q2	0.396629	0.397572	0.043044	0.040533	0.036175	0.034646
Q3	0.162133	0.145500	0.120709	0.106719	0.303075	0.295050
Q4	0.280676	0.280975	0.151627	0.145669	0.133883	0.131968
TA = 15° C, R = 1 cm						
Q1	0.227928	0.188492	0.141034	0.109312	**0.984172**	0.952563
Q2	0.898900	0.898802	0.067610	0.063170	0.056295	0.054221
Q3	0.357879	0.319596	0.267523	0.240491	0.592053	0.573809
Q4	0.548922	0.548305	0.322320	0.308006	0.282986	0.280491
TA = 15° C, R = 2 cm						
Q1	0.454763	0.360672	0.264323	0.197095	**2.684084**	2.569004
Q2	2.423443	2.368025	0.053276	0.047718	0.041156	0.037929
Q3	0.823447	0.725776	0.612409	0.552633	1.038416	0.998494
Q4	0.963543	0.969501	0.709299	0.669590	0.617098	0.602305

Table 4 TDE deviation $D_{MAX}{}^{M}$ in M = CTM at $T_A = 25°$ C. Maximum value for fixed R and fixed SP_Rk: light grey, maximum value for fixed R over all SP_Rk: fat print, dark grey

TDE deviation – CTM model - D_{MAX}						
TA = 25° C, R = 0.5 cm						
	SP5	SP3	SP1	SP6	SP4	SP2
Q1	0.096924	0.087224	0.064009	0.047629	**0.478770**	0.472093
Q2	0.433839	0.420362	0.044949	0.043581	0.038244	0.035446
Q3	0.155922	0.146795	0.119631	0.102337	0.336467	0.331520
Q4	0.305825	0.297609	0.163489	0.160196	0.144541	0.137588
TA = 25° C, R = 1 cm						
Q1	0.200676	0.176616	0.127789	0.093306	**1.085921**	1.064973
Q2	0.978343	0.949218	0.070626	0.067887	0.059601	0.055385
Q3	0.348042	0.325264	0.267879	0.232388	0.657130	0.643892
Q4	0.594666	0.580189	0.347716	0.338657	0.305722	0.291640
TA = 25° C, R = 2 cm						
Q1	0.401715	0.336522	0.240250	0.171164	**2.953641**	2.854130
Q2	2.631010	2.552613	0.054170	0.050111	0.042954	0.038911
Q3	0.813108	0.743778	0.622384	0.548695	1.153148	1.114621
Q4	1.035954	1.013757	0.765055	0.732501	0.663553	0.634064

Table 5 TDE deviation $D_{MAX}{}^{M}$ in M = CMS at $T_A = 5°$ C. Maximum value for fixed R and fixed SP_Rk: light grey, maximum value for fixed R over all SP_Rk: fat print, dark grey

TDE deviation – CMS model - D_{MAX}						
TA = 5° C, R = 0.5 cm						
	SP5	SP3	SP1	SP6	SP4	SP2
Q1	0.278668	0.428958	0.036924	0.335980	**0.499407**	0.036924
Q2	0.237840	0.249328	0.034020	0.287842	0.348655	0.034020
Q3	0.187893	0.116238	0.029856	0.228624	0.222521	0.029856
Q4	0.154688	0.074618	0.027514	0.190183	0.145349	0.027514
TA = 5° C, R = 1 cm						
Q1	0.554121	0.847941	0.073925	0.676501	**1.002985**	0.073925
Q2	0.459769	0.466711	0.066970	0.564490	0.663992	0.066970
Q3	0.363333	0.208421	0.059023	0.449124	0.421534	0.059023
Q4	0.298674	0.161567	0.054472	0.373160	0.273236	0.054472
TA = 5° C, R = 2 cm						
Q1	1.095381	1.563284	0.176399	1.371045	**1.999290**	0.176399
Q2	0.860177	0.756267	0.154756	1.086690	1.247146	0.154756
Q3	0.682823	0.273074	0.137774	0.868890	0.800136	0.137774
Q4	0.557965	0.424460	0.127253	0.719497	0.524725	0.127253

Table 6 TDE deviation $D_{MAX}{}^{M}$ in M = CMS at $T_A = 15°$ C. Maximum value for fixed R and fixed SP_Rk: light grey, maximum value for fixed R over all SP_Rk: fat print, dark grey

TDE deviation – CMS model - D_{MAX}						
TA = 15° C, R = 0.5 cm						
	SP5	SP3	SP1	SP6	SP4	SP2
Q1	0.267230	0.357906	0.037319	0.322041	**0.439618**	0.037319
Q2	0.247672	0.240927	0.036283	0.299441	0.353170	0.036283
Q3	0.196644	0.114936	0.031731	0.239472	0.230824	0.031731
Q4	0.158513	0.073921	0.028449	0.194800	0.149584	0.028449
TA = 15° C, R = 1 cm						
Q1	0.531431	0.717470	0.074719	0.648396	**0.881242**	0.074719
Q2	0.482692	0.458454	0.071888	0.592171	0.682468	0.071888
Q3	0.380752	0.209685	0.062621	0.471052	0.440656	0.062621
Q4	0.307615	0.158411	0.056403	0.384086	0.284623	0.056403
TA = 15° C, R = 2 cm						
Q1	1.050738	1.369435	0.178258	1.313951	**1.804971**	0.178258
Q2	0.915332	0.762669	0.167574	1.155611	1.314195	0.167574
Q3	0.715042	0.285432	0.145382	0.911878	0.848165	0.145382
Q4	0.579908	0.414947	0.132116	0.746680	0.559106	0.132116

Table 7 TDE deviation $D_{MAX}{}^{M}$ in M = CMS at $T_A = 25°$ C. Maximum value for fixed R and fixed SP_Rk: light grey, maximum value for fixed R over all SP_Rk: fat print, dark grey

TDE deviation – CMS model - D_{MAX}						
TA = 25° C, R = 0.5 cm						
	SP5	SP3	SP1	SP6	SP4	SP2
Q1	0.262335	0.305714	0.037699	0.315216	**0.395636**	0.037699
Q2	0.246257	0.194035	0.036956	0.296862	0.319504	0.036956
Q3	0.201215	0.085054	0.033200	0.244457	0.214002	0.033200
Q4	0.168303	0.085014	0.030656	0.206545	0.144324	0.030656
TA = 25° C, R = 1 cm						
Q1	0.521653	0.610921	0.075482	0.634763	0**.792969**	0.075482
Q2	0.482290	0.371160	0.073451	0.589914	0.621087	0.073451
Q3	0.393083	0.155605	0.065927	0.484524	0.413476	0.065927
Q4	0.327041	0.179284	0.060712	0.408028	0.276591	0.060712
TA = 25° C, R = 2 cm						
Q1	1.031287	1.148291	0.180043	1.286870	**1.631598**	0.180043
Q2	0.923440	0.610350	0.172432	1.163235	1.221785	0.172432
Q3	0.751407	0.193555	0.154966	0.953344	0.821985	0.154966
Q4	0.617182	0.448666	0.141694	0.796183	0.555555	0.141694

Table 8 TDE deviation $D_{MAX}{}^{M}$ in M = CM at $T_A = 5°$ C. Maximum value for fixed R and fixed SP_Rk: light grey, maximum value for fixed R over all SP_Rk: fat print, dark grey

TDE deviation – CM model - D_{MAX}						
TA = 5° C, R = 0.5 cm						
	SP5	SP3	SP1	SP6	SP4	SP2
Q1	0.200747	0.082531	0.027118	0.234452	**0.058478**	0.027118
Q2	0.167312	0.075431	0.024499	0.198540	0.052605	0.024499
Q3	0.147537	0.072658	0.023330	0.177736	0.049917	0.023308
Q4	0.132639	0.071803	0.022760	0.162265	0.048585	0.022760
TA = 5° C, R = 1 cm						
Q1	0.398077	0.165600	0.054291	0.471954	**0.117226**	0.054291
Q2	0.330775	0.151129	0.048947	0.398347	0.105220	0.048947
Q3	0.291018	0.145433	0.046554	0.355941	0.099732	0.046554
Q4	0.261757	0.143978	0.045487	0.324939	0.097223	0.045487
TA = 5° C, R = 2 cm						
Q1	0.781054	0.393109	0.129297	0.954274	**0.284217**	0.129297
Q2	0.647372	0.357693	0.116338	0.802568	0.255143	0.116338
Q3	0.566684	0.343067	0.110378	0.713686	0.241735	0.110378
Q4	0.509666	0.340011	0.108049	0.651276	0.236595	0.108049

Table 9 TDE deviation $D_{MAX}{}^{M}$ in M = CM at $T_A = 15°$ C. Maximum value for fixed R and fixed $SP_R k$: light grey, maximum value for fixed R over all $SP_R k$: fat print, dark grey

TDE deviation – CM model - D_{MAX}						
TA = 15° C, R = 0.5 cm						
	SP5	SP3	SP1	SP6	SP4	SP2
Q1	0.197012	0.089669	0.028232	0.231895	**0.058956**	0.028232
Q2	0.175701	0.083939	0.026275	0.208845	0.054782	0.026275
Q3	0.150650	0.077918	0.024152	0.181378	0.050239	0.024152
Q4	0.133215	0.075424	0.023037	0.162939	0.047882	0.023037
TA = 15° C, R = 1 cm						
Q1	0.391470	0.179959	0.056522	0.467431	**0.118182**	0.056522
Q2	0.346627	0.167844	0.052371	0.418501	0.109343	0.052371
Q3	0.297808	0.156149	0.048259	0.363749	0.100499	0.048259
Q4	0.262909	0.151386	0.045997	0.326199	0.095721	0.045997
TA = 15° C, R = 2 cm						
Q1	0.772885	0.425441	0.134783	0.949703	**0.289311**	0.134783
Q2	0.675116	0.393752	0.123877	0.840604	0.265806	0.123877
Q3	0.582480	0.367737	0.114700	0.731941	0.245890	0.114700
Q4	0.513395	0.356835	0.109293	0.654243	0.234786	0.109293

Table 10 TDE deviation $D_{MAX}{}^{M}$ in M = CM at $T_A = 25°$ C. Maximum value for fixed R and fixed SP_Rk: light grey, maximum value for fixed R over all SP_Rk: fat print, dark grey

TDE deviation – CM model - D_{MAX}						
TA = 25° C, R = 0.5 cm						
	SP5	SP3	SP1	SP6	SP4	SP2
Q1	0.208154	0.103755	0.031377	0.246592	**0.063438**	0.031377
Q2	0.197806	0.101076	0.030469	0.235852	0.061586	0.030469
Q3	0.163070	0.088843	0.026560	0.196638	0.053675	0.026560
Q4	0.142644	0.083820	0.024782	0.174261	0.050165	0.024782
TA = 25° C, R = 1 cm						
Q1	0.413721	0.208270	0.062820	0.496892	**0.127163**	0.062820
Q2	0.390814	0.202239	0.060775	0.473168	0.123023	0.060775
Q3	0.321978	0.177811	0.052972	0.394433	0.107212	0.052972
Q4	0.281984	0.168014	0.049502	0.349622	0.100351	0.049502
TA = 25° C, R = 2 cm						
Q1	0.817206	0.490223	0.149801	1.008790	**0.313927**	0.149801
Q2	0.762105	0.472764	0.143783	0.952108	0.301548	0.143783
Q3	0.627905	0.415840	0.125489	0.793106	0.263418	0.125489
Q4	0.551370	0.393797	0.117604	0.703184	0.247701	0.117604

Supplementary information The online version contains supplementary material available at https://doi.org/10.1007/s00414-023-03040-y.

Acknowledgements The present study is part of a project funded by the Deutsche Forschungsgemeinschaft DFG with the reference numbers MA 2501/4-1 (Prof. Dr. Gita Mall) and WE 2937/10-1 (Dr. Martin Weiser).

Authors contributions Study design and milestone discussions: All authors. CT-segmentation: ZIB authors. FE model CTM generation: ZIB authors, CTM migration: All authors. CMS generation: IRM authors. FE computations: J. Ulrich, J. Shanmugam, H. Muggenthaler. Distance measure computations: J. Shanmugam, M. Hubig. Output interpretation/presentation: J. Shanmugam, M. Hubig, H. Muggenthaler, J. Ulrich. Paper written/corrected: J. Shanmugam, M. Hubig, H. Muggenthaler. Paper reading / corrections: All authors.

Funding Open Access funding enabled and organized by Projekt DEAL.

Material and/or code availability The individual CT scan used in the current study is not publicly available. Each single slice is linked to a DICOM-file containing experiment parameter data and sensible case information. The program code is available from the corresponding author on reasonable request.

Declarations

Ethical approval No living or deceased humans nor living or dead animals were directly involved in the study. Written consents of the CTM-subject's kinship for the CT scan shown in the article were not needed since the body was confiscated by the local prosecution who directed the CT scan for investigations.

Competing interests The authors herewith disclose financial or non-financial interests that are directly or indirectly related to the work.

References

1. Henßge C (2016) 6.1 Basics and application of the 'nomogram method' at the scene. In: Madea B (ed) (2016) Estimation of the Time Since Death, 3rd edn. CNC Press Taylor & Francis Routledge, Boca Raton FL
2. Mall G, Eisenmenger W (2005) Estimation of time since death by heat-flow Finite-Element model. Part I: method, model, calibration and validation. Leg Med 7(1):1–14. https://doi.org/10.1016/j.legalmed.2004.06.006
3. Mall G, Eisenmenger W (2005) Estimation of time since death by heat-flow Finite-Element model part II: application to non-standard cooling conditions and preliminary results in practical casework. Leg Med 7(2):69–80. https://doi.org/10.1016/j.legalmed.2004.06.007
4. Schenkl S, Muggenthaler H, Hubig M, Erdmann B, Weiser M, Zachow S, Heinrich A, Güttler F, Teichgräber U, Mall G (2017) Automatic CT-based finite element model generation for temperature-based death time estimation: feasibility study and sensitivity analysis. Intl J Leg Med 131(3):699–712. https://doi.org/10.1007/s00414-016-1523-0
5. Madea B (ed) (2016) Estimation of the Time Since Death, 3rd edn. CNC Press Taylor & Francis Routledge, Boca Raton FL
6. Hubig M, Muggenthaler H, Mall G (2011) Influence of measurement errors on temperature-based death time determination. Int J Legal Med 125:503–517. https://doi.org/10.1007/s00414-010-0453-5
7. Weiser M, Erdmann B, Schenkl S, Muggenthaler H, Hubig M, Mall G, Zachow S (2018) Uncertainty in temperature-based determination of time of death. Heat Mass Transf 54:2815–2826. https://doi.org/10.1007/s00231-018-2324-4
8. De Saram GSW, De Webster G, Kathirgamatamby N (1955) Post-mortem temperature and the time of death. J Crim Law Criminol 46(2):562–577
9. Marshall TK, Hoare FE (1962) Estimating the time of death. The rectal cooling after death and its mathematical expression. J Forensic Sci 7:56–81
10. Marshall TK, Hoare FE (1962) Estimating the time of death. The use of the cooling formula in the study of post-mortem body cooling. J Forensic Sci 7:189–210
11. Henßge C (1979) Die Präzision von Todeszeitschätzungen durch die mathematische Beschreibung der rektalen Leichenabkühlung. Z Rechtsmedizin 83:49–67
12. Henßge C, Madea B (1988) Methoden zur Bestimmung der Todeszeit an Leichen, 1st edn. Schmidt-Römhild, Lübeck, Verlag Schmidt-Römhild, Lübeck, Germany, p 288
13. Henßge C, Brinkmann B, Püschel K (1984) Todeszeitbestimmung durch Rektaltemperaturmessungen bei Wassersuspension der Leiche. Z Rechtsmedizin 92:255–276. https://doi.org/10.1007/BF00200284
14. Henßge C (1981) Todeszeitschätzungen durch die mathematische Beschreibung der rektalen Leichenabkühlung unter verschiedenen Abkühlbedingungen. Z Rechtsmedizin 87:147–178
15. Henßge C (2002) Todeszeitbestimmung an Leichen. Rechtsmedizin 12:112–131. https://doi.org/10.1007/s00194-002-0136-8
16. Deuflhard P, Weiser M (2012) Adaptive numerical solution of PDEs. De Gruyter, Berlin
17. Hubig M, Muggenthaler H, Mall G (2016) 6.2 Finite element method in temperature-based death time determination. In: Madea B (ed) (2016) Estimation of the Time Since Death, 3rd edn. CNC Press Taylor & Francis Routledge, Boca Raton FL
18. Pennes HH (1948) Analysis of tissue and arterial blood temperatures in the resting human forearm. J Appl Physiol 1(2):93–122. https://doi.org/10.1152/jappl.1948.1.2.93
19. Götschel S, Schiela A, Weiser M (2021) Kaskade 7 - a flexible finite element toolbox. Comp Math Appl 81:444–458. https://doi.org/10.1016/j.camwa.2020.02.011

20. Muggenthaler H, Hubig M, Schenkl S, Mall G (2017) Influence of hypo- and hyperthermia on death time estimation - A simulation study. Leg Med 28:10–14. https://doi.org/10.1016/j.legalmed.2017.06.005
21. Muggenthaler H, Hubig M, Schenkl S, Niederegger S, Mall G (2017) Calibration and parameter variation using a finite element model for death time estimation: the influence of the substrate. Leg Med 25:23–28. https://doi.org/10.1016/j.legalmed.2016.12.007
22. Cengel YA, Ghajar AJ (2014) Heat and Mass Transfer – Fundamentals and Applications, 5th edn. McGraw-Hill, New York
23. Gray H (1918) Anatomy of Human Body, 1st edn. Lea & Febiger, Philadelphia, Retrieved from Library of Congress. https://lccn.loc.gov/18017427. Accessed 17 Oct 2022
24. Baumann F (2020) Impact of contact surfaces on the death estimation. Master Thesis, Technische Universität Berlin, p 69